LANGMUIR

pubs.acs.org/Langmuir Article

Rapid and Onsite Detection of Fuel Adulteration

Sanli Movafaghi, Sravanthi Vallabhuneni, Wei Wang, Shantanu Jathar, and Arun K. Kota*

Cite This: *Langmuir* 2023, 39, 9044−9050 Read Online

ACCESS | Metrics & More | Article Recommendations | Supporting Information

ABSTRACT: In numerous developing countries, the lower cost of subsidized liquid fuels such as kerosene compared to market-rate fuels often results in fuel adulteration. Such misuse of kerosene is hard to detect with conventional detection technologies because they are either time consuming, expensive, not sensitive enough or require well-equipped analytical laboratories. In this work, we developed an inexpensive and easy-to-use device for rapid and onsite detection of fuel adulteration. The working principle of our fuel adulteration detection is sensing changes in the mobility of fuel droplets on non-textured (i.e., smooth) and non-polar solid surfaces. Using our device, we demonstrated rapid detection of diesel (market-rate fuel) adulterated with kerosene (subsidized fuel) at concentrations an order of magnitude below typical adulteration concentrations. We envision that our inexpensive, easy-to-use, and field-deployable device as well as the design strategy will pave the way for novel fuel quality sensors.

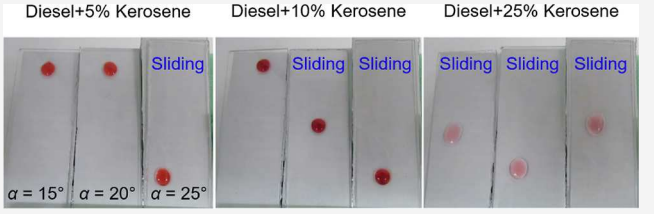

INTRODUCTION

Numerous developing countries in Asia (e.g., India) and Africa (e.g., Nigeria) offer subsidized liquid fuels such as kerosene to support lighting and cooking needs of the rural poor.[1−3] The low cost of kerosene compared to market-rate fuels often results in fuel adulteration, i.e., the unauthorized addition of foreign substance into fuel. For example, about 40% of the kerosene sold in India frequently gets blended with gasoline and diesel.[4−6] Such fuel adulteration can be as high as 35−50%, and it significantly alters the desired properties of the fuel and leads to substantial economic and environmental concerns.[4,6−10] Thus far, onsite (e.g., at fuel dispensing stations) detection of fuel adulteration with kerosene has been difficult to quantify because the existing technologies for detecting fuel adulteration (e.g., gas chromatography−mass spectrometry, Fourier transform infrared spectrometry, microcontroller sensor, long period fiber grating, hydrometer, etc.) are either time consuming, expensive, not sensitive enough or require well-equipped analytical laboratories.[6,11−13] So, there is a critical need for inexpensive and easy-to-use devices for rapid and onsite detection of fuel adulteration, especially in developing economies, where fuel quality is a major concern. In this work, we developed an inexpensive and easy-to-use device for rapid and onsite detection of fuel adulteration using smooth and non-polar surfaces. Our device detects fuel adulteration by sensing changes in the mobility of a fuel droplet on a solid surface that in turn depends on the surface tension of the fuel. We have rationally designed our device so that it can detect changes in the mobility of the fuel droplet even at concentrations an order of magnitude below typical adulteration concentrations. We envision that our inexpensive, easy-to-use, and field-deployable device as well as the design strategy will pave the way for novel fuel quality sensors.

The working principle of our fuel adulteration detection is identifying the changes in mobility of fuel droplets on a solid surface. One simple measure of the mobility of a fuel droplet on a solid surface is the sliding angle ω (i.e., the minimum angle by which the surface must be tilted relative to the horizontal for a liquid droplet to slide off from the surface). Sliding angle ω can be estimated based on a balance between work done by gravitational force and work expended due to adhesion as[14−21]

$$\rho g V \sin \omega \approx \gamma_{lv} D_{TCL} (\cos \theta_{rec} - \cos \theta_{adv}) \quad (1)$$

Here, D_{TCL} is the width of solid−liquid−vapor contact line perpendicular to the sliding direction, γ_{lv} and ρ are the surface tension and density of the liquid, respectively, g is the acceleration due to gravity, V is the volume of the liquid droplet, θ_{adv} is the advancing (maximum) contact angle, and θ_{rec} is the receding (minimum) contact angle. Typically, droplets of low surface tension liquids (e.g., alkanes, alcohols etc.) display low sliding angles on non-textured (i.e., smooth) and non-polar solid surfaces.[22,23] Now, let us consider alkane droplets of a constant volume V on non-textured and non-polar solid surfaces. An alkane droplet with a lower surface tension $\gamma_{lv,low}$ displays lower sliding angle ω_{low}, and an alkane droplet with a higher surface tension $\gamma_{lv,high}$ displays higher sliding angle ω_{high} (i.e., for $\gamma_{lv,low} < \gamma_{lv,high}$, $\omega_{low} < \omega_{high}$). When the droplets of both lower and higher surface tension alkanes are placed on a solid surface, for a tilt angle $\alpha < \omega_{low}$, both the alkane droplets remain adhered to

Received: March 1, 2023
Revised: May 31, 2023
Published: June 16, 2023

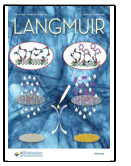

https://doi.org/10.1021/acs.langmuir.3c00578
Langmuir 2023, 39, 9044−9050

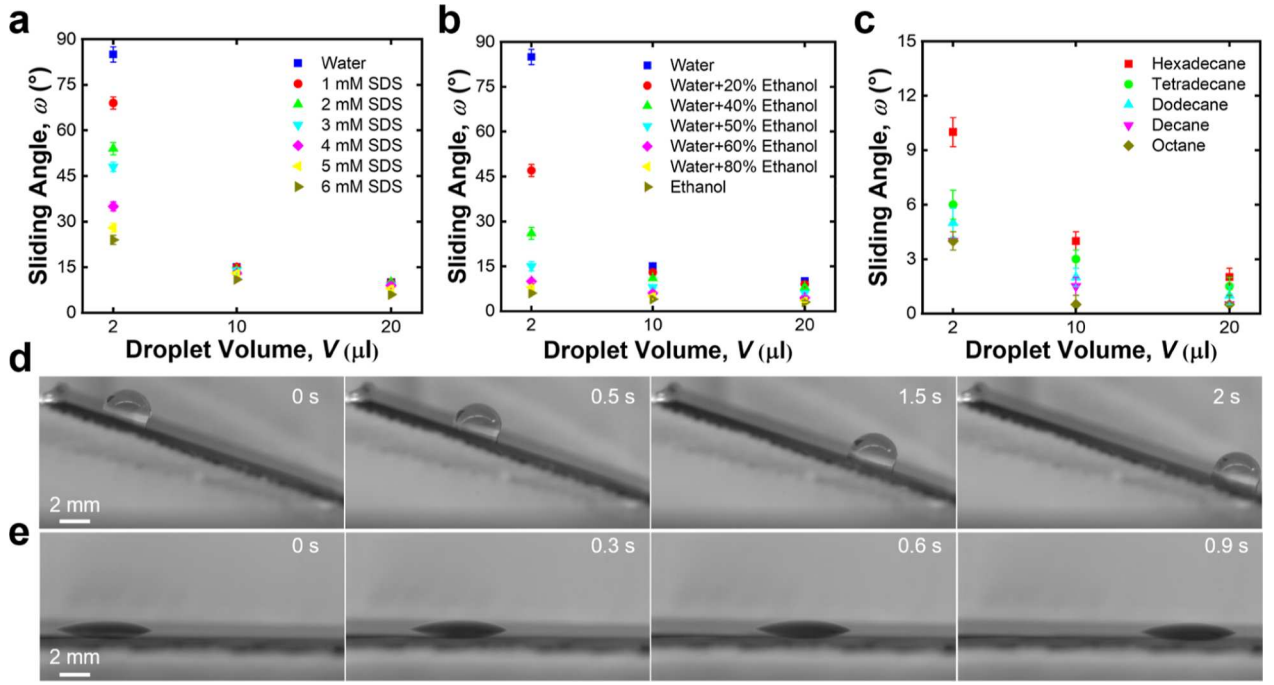

Figure 1. Droplet mobility on OTS-modified silicon wafers. Sliding angles of (a) water−SDS mixtures, (b) water−ethanol mixtures, and (c) homologous series of alkanes as a function of droplet volume. All sliding angle measurements were conducted on at least three different samples, and the standard deviation is reported as the error in the data. (d) Series of images demonstrating a 10 μL water droplet sliding on OTS-modified silicon wafer titled at 20°. (e) Series of images demonstrating a 10 μL *n*-decane droplet sliding on OTS-modified silicon wafer titled at 2°.

the surface with no motion; for $\omega_{low} < \alpha < \omega_{high}$, the alkane droplet with lower surface tension $\gamma_{lv,low}$ slides past the surface, but the alkane droplet with higher surface tension $\gamma_{lv,high}$ remains adhered to the surface; and for $\alpha > \omega_{high}$, both the alkane droplets slide past the surface. In a similar manner, consider droplets of a fuel blend (predominantly consisting of alkanes) with a constant volume V. The sliding angle of a fuel blend droplet decreases with decreasing surface tension, which in turn depends on its chemical composition. When a market-rate fuel (e.g., diesel with γ_{lv} = 25.8 mN m^{-1}) is adulterated by blending with another subsidized fuel (e.g., kerosene with γ_{lv} = 20.1 mN m^{-1}), its chemical composition and consequently its surface tension changes. Correspondingly, the sliding angle of the adulterated fuel blend changes compared to the unadulterated fuel. Leveraging such differences in sliding angles of fuel blend droplets, we designed our device to detect fuel adulteration.

RESULTS AND DISCUSSION

To systematically design a fuel adulteration detection device, we first studied the mobility of droplets on non-textured (i.e., smooth) substrates with different non-polar (hydrocarbon and fluorocarbon) chemistries. To begin with, we chose silicon wafers (R_{rms} = 1.4 ± 0.5 nm) as our non-textured substrates because they display low surface roughness, and they can be easily modified via silanization to impart non-polar surface chemistry.[24] We modified the surface chemistry of silicon wafers by covalently attaching hydrocarbon brushes (with octadecyltrichlorosilane, OTS, thickness ≈ 1 nm) or fluorocarbon brushes (with heptadecafluoro-1,1,2,2-tetrahydrodecyl trichlorosilane, FDTS, thickness ≈ 1 nm) via liquid phase silanization; the surface roughness R_{rms} of silicon wafers did not change significantly upon surface modification with OTS or FDTS (see Supporting Information, Section S1). We chose two different non-polar surface chemistries to investigate because we anticipate that the differences in chain flexibility of hydrocarbon and fluorocarbon brushes will influence the mobility of droplets,[22,25] which plays a critical role in designing our fuel adulteration detection device. Typically, hydrocarbon brushes display higher chain flexibility compared to their fluorocarbon analogues, resulting in higher droplet mobility on a solid surface.[26−30] We characterized the surface chemistry of our unmodified, OTS-modified, and FDTS-modified silicon wafers using X-ray photoelectron spectroscopy (see Supporting Information, Section S2).

We investigated the mobility of droplets on OTS-modified and FDTS-modified silicon wafers using multiple liquid systems [i.e., water−sodium dodecyl sulfate (SDS) mixtures, water−ethanol mixtures, and homologous series of alkanes] by measuring sliding angles as a function of droplet volume. Our OTS-modified silicon wafers displayed high droplet mobility (see Figure 1a−c and see Supporting Information, Section S3) with both high surface tension liquids (e.g., water, γ_{lv} = 72 mN m^{-1}, see Figure 1d) and low surface tension liquids (e.g., *n*-decane, γ_{lv} = 20 mN m^{-1}, see Figure 1e). For each liquid, as the droplet volume decreased, the sliding angles increased (i.e., droplet mobility decreased), in accordance with eq 1.[31,32] More importantly, for any two liquids within each liquid system (i.e., water−SDS mixtures, water−ethanol mixtures, or homologous series of alkanes), as the droplet volume decreased, the difference in droplet sliding angles increased (see Figure 1a−c and Table S1). This indicates that lower droplet volumes allow for more noticeable differences in droplet mobility between any two liquids studied (even with small changes in surface tension or composition) within a liquid system. For example, on OTS-modified silicon wafers, at 20 μL droplet volume, the sliding angles of water−SDS system spanned across a range of 4° (i.e., difference in droplet sliding angles of water and water + 6 mM SDS). When the droplet volume decreased to 2 μL, this range in

https://doi.org/10.1021/acs.langmuir.3c00578
Langmuir 2023, 39, 9044−9050

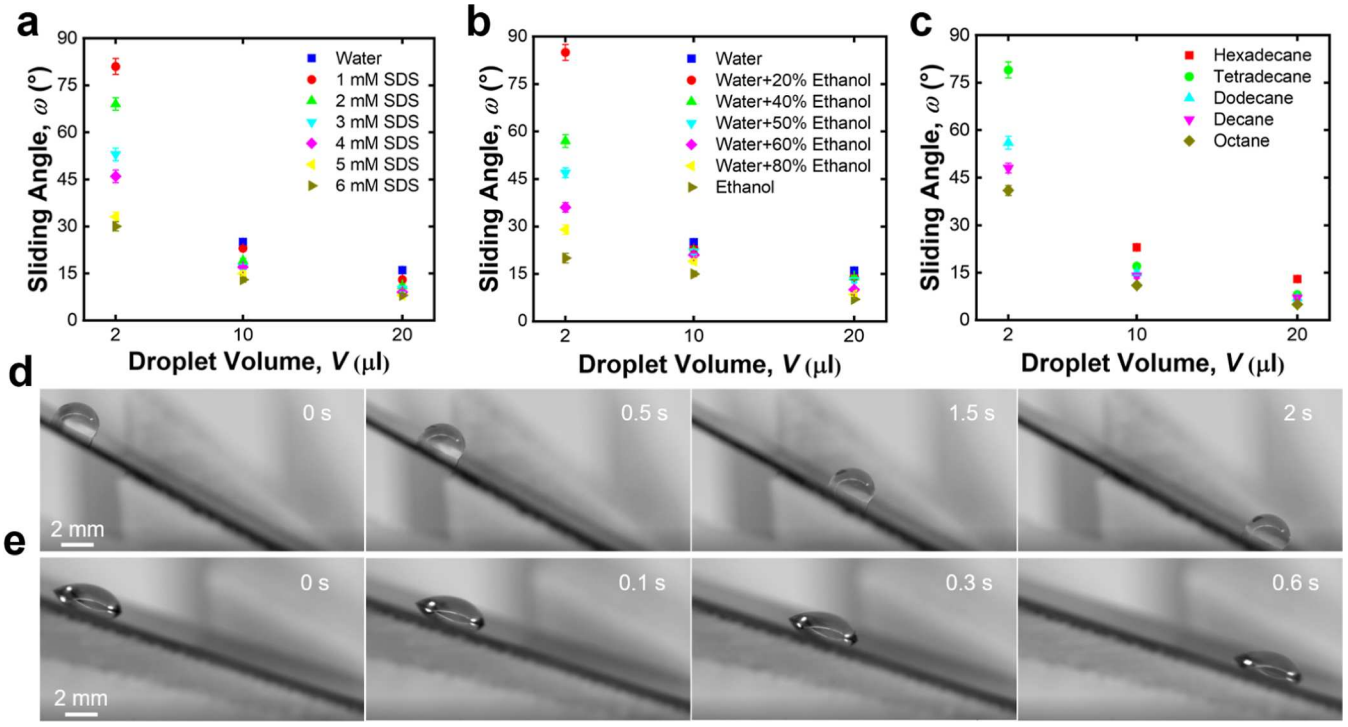

Figure 2. Droplet mobility on FDTS-modified silicon wafers. Sliding angles of (a) water−SDS mixtures, (b) water−ethanol mixtures, and (c) homologous series of alkanes as a function of droplet volume. The sliding angles of 2 μL water droplets in the plots (a,b) and 2 μL hexadecane droplets in the plot (c) were not reported because they were not sliding even at 90° on FDTS-modified silicon wafers due to their low liquid volumes. All sliding angle measurements were conducted on at least three different samples, and the standard deviation is reported as the error in the data. (d) Series of images demonstrating a 10 μL water droplet sliding on FDTS-modified silicon wafer titled at 30°. (e) Series of images demonstrating a 10 μL *n*-decane droplet sliding on FDTS-modified silicon wafer titled at 20°.

sliding angles increased to 61° (see Figure 1a). Similar increasing trend in the range of sliding angles with decreasing droplet volume was also observed with the water−ethanol system (see Figure 1b) and alkanes (see Figure 1c). Such higher ranges in sliding angles indicate that the changes in droplet mobility are more distinct at lower droplet volumes for each liquid system. This in turn allows sensing changes in the liquid composition at finer levels of adulteration enabling reliable detection.

Our FDTS-modified silicon wafers also displayed high droplet mobility (see Figure 2a−c and see Supporting Information, Section S3) with both high surface tension liquids (e.g., water, see Figure 2d) and low surface tension liquids (e.g., *n*-decane, see Figure 2e). As anticipated, all liquids also displayed increasing sliding angles (i.e., decreasing droplet mobility) with decreasing the droplet volume. The sliding angles on FDTS-modified silicon wafers were slightly higher compared to OTS-modified silicon wafers. For example, a 20 μL water droplet displayed a sliding angle of 16° on FDTS-modified silicon wafer (see Figure 2a) and 10° on OTS-modified silicon wafer (see Figure 1a). This increase in the sliding angle (i.e., decrease in droplet mobility) is due to the lower chain flexibility of FDTS brushes compared to OTS brushes on modified silicon wafers.[22,25−28,30] Similar to the OTS-modified silicon wafers, FDTS-modified silicon wafers also displayed an increasing trend in the range of sliding angles with decreasing droplet volume for each liquid system (see Figure 2a−c and Table S1). This reaffirms that difference in droplet mobility is more distinct at lower droplet volumes, which enables reliable fuel adulteration detection. Overall, our droplet mobility results on OTS-modified silicon wafers (see Figure 1) and FDTS-modified silicon wafers (see Figure 2) indicate that either of these nonpolar surface chemistries is suitable for designing a fuel adulteration detection device when lower droplet volumes are used. For example, for 2 μL droplets on OTS-modified silicon wafers, comparing the sliding angles of water + 50% ethanol (15°) with those of water (85°) and ethanol (6°) clearly indicates the presence of ethanol in water (see Figure 1b). Similarly, for 2 μL droplets on FDTS-modified silicon wafers, comparing the sliding angles of water + 50% ethanol (47°) with those of water (no sliding) and ethanol (20°) clearly indicates the presence of ethanol in water (see Figure 2b).

While we could have used FDTS-modified substrates to design our device for detecting fuel adulteration, we chose to use OTS-modified substrates because hydrocarbon ligands are environmentally friendly compared to their fluorocarbon analogues, which have raised worldwide environmental concerns.[33−35] To develop a device that can detect the adulteration of diesel with kerosene, we first characterized the droplet mobility of diesel−kerosene blends on OTS-modified silicon wafers as a function of blend concentration and droplet volume (see Figure 3a). As the kerosene concentration in the diesel−kerosene blend varied from 0% (only diesel) to 100% (only kerosene) by volume, the surface tension of the blend varied from 25.8 to 20.1 mN m^{-1} (see Supporting Information, Section S4). As anticipated, our OTS-modified silicon wafers displayed lower sliding angles with higher kerosene concentrations (i.e., lower surface tension blends; see Figure 3a and Supporting Information, Section S4), indicating higher droplet mobility with increasing kerosene concentration in the blend. However, the sliding angle differences across the diesel−kerosene blends were too low. For example, 5 μL droplets of

https://doi.org/10.1021/acs.langmuir.3c00578
Langmuir 2023, 39, 9044−9050

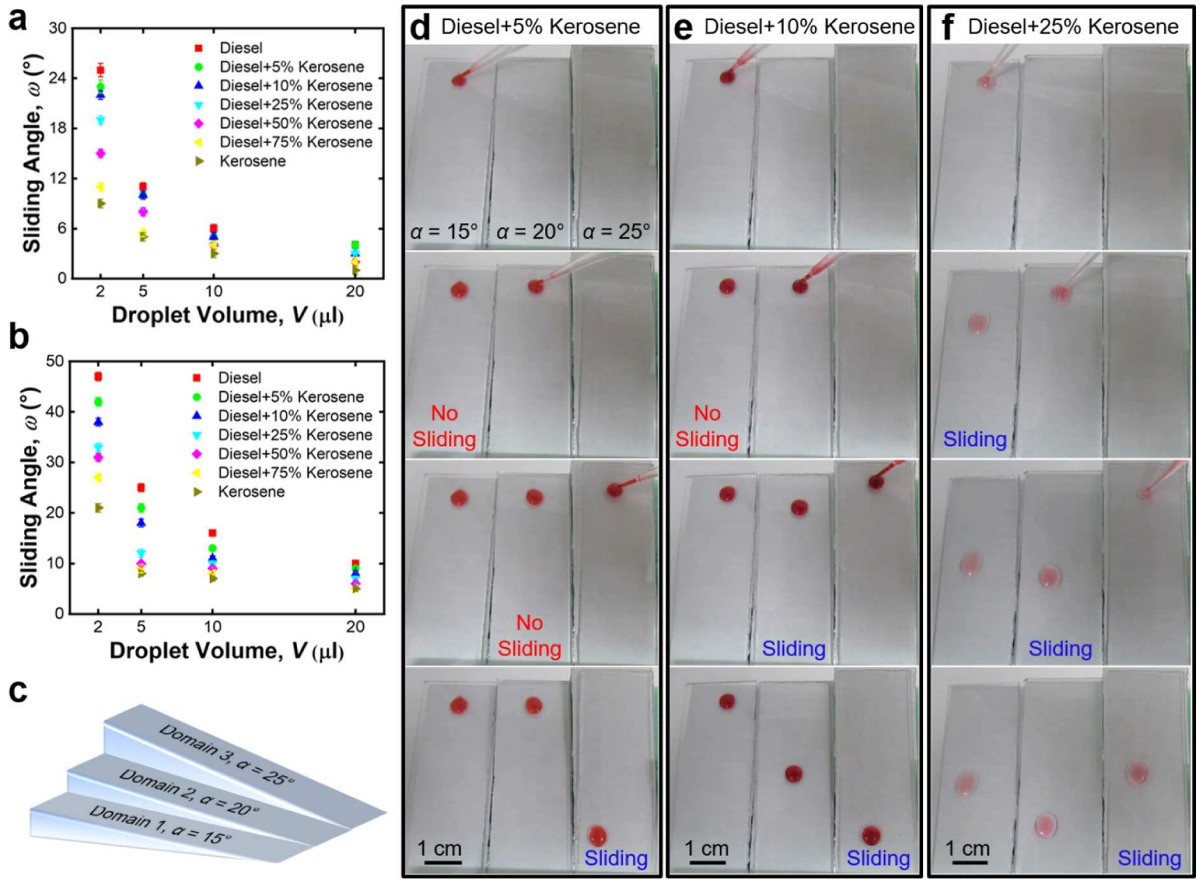

Figure 3. Droplet mobility of diesel−kerosene blends on OTS-modified surfaces. Sliding angles of diesel−kerosene blends on (a) OTS-modified silicon wafers and (b) OTS-modified glass slides as a function of droplet volume. All sliding angle measurements were conducted on at least three different samples, and the standard deviation is reported as the error in the data. (c) Schematic depicting three domains at 15, 20, and 25° tilt angles. Series of images illustrating the mobility with 5 μL droplets of (d) diesel + 25% kerosene blend, (e) diesel + 10% kerosene blend, and (f) diesel + 5% kerosene blend on OTS-modified glass slides at different tilt angles (15, 20, and 25°).

diesel and diesel + 10% kerosene displayed sliding angles of 11 and 10°, respectively, on OTS-modified silicon wafers. Such low differences in sliding angles make it practically difficult to detect changes in mobility due to changes in the composition, thereby leading to unreliable detection.

To obtain larger differences in droplet sliding angles across diesel−kerosene blends on OTS-modified surfaces, we used glass slides, which have higher surface roughness (R_{rms} = 5.2 ± 1.3 nm) compared to silicon wafers. We projected that the higher surface roughness of OTS-modified glass slides will result in higher contact angle hysteresis,[36−38] which in turn may magnify the differences in droplet sliding angles across diesel−kerosene blends (see Supporting Information, Section S5), thereby allowing reliable detection of adulteration. Furthermore, compared to silicon wafers, glass slides are inexpensive, which makes our device cost-effective and improves its scalability. Indeed, our OTS-modified glass slides displayed a wider range in the sliding angles across the diesel−kerosene blends (see Figure 3b and Table S2) at all droplet volumes compared to OTS-modified silicon wafers (see Figure 3a and Table S2). For example, 5 μL droplets of diesel and diesel + 10% kerosene displayed sliding angles of 25 and 18°, respectively, on OTS-modified glass slides. This indicates a significantly larger difference in the droplet sliding angles on rougher OTS-modified glass substrates compared to smoother OTS-modified silicon substrates. Such larger differences in sliding angles across diesel−kerosene blends will produce more noticeable changes in droplet mobility. In turn, this reduces the error and allows for reliable detection of diesel adulteration by kerosene.

Based on the droplet mobility results of diesel−kerosene blends on OTS-modified glass slides, we fabricated a simple, inexpensive, and field-deployable device using 3D printing (see Supporting Information, Section S6 and Figure S3) to demonstrate rapid fuel adulteration detection. Our fuel adulteration detection device consists of multiple wedges that can accommodate OTS-modified substrates at a wide variety of tilt angles α (see Figures 3c and S3). When liquid droplets of an unknown composition (diesel or diesel−kerosene blends) and same volume are placed on wedges with different tilt angles α, the droplets would remain adhered when sliding angle $\omega > \alpha$ and the droplets would slide when the sliding angle $\omega < \alpha$. As demonstrated previously (see Figure 3a,b), for diesel−kerosene blends, the sliding angle ω decreases with increasing kerosene concentration (i.e., droplet mobility increases with increasing adulteration). So, by placing droplets of a diesel−kerosene blend with unknown composition and fixed volume on wedges with different tilt angles and identifying the mobility of the droplet (i.e., the tilt angle at which the droplet slides) and comparing it with the sliding angles of diesel−kerosene blends on OTS substrates (see Figure 3b), we can estimate the composition diesel−kerosene blend. To demonstrate this (see Figure 3d−f), we used 5 μL droplets of different diesel−kerosene blends on our device with wedges having 15, 20, and 25° tilt angles. We chose 5 μL droplets of diesel−kerosene blends because they not

https://doi.org/10.1021/acs.langmuir.3c00578
Langmuir 2023, 39, 9044−9050

only displayed a sufficiently large difference in sliding angles (i.e., 17° difference between diesel and kerosene) but also displayed sufficiently large sliding velocities. Unlike 5 μL droplets, 20 μL droplets displayed low differences in sliding angles (i.e., 5° difference between diesel and kerosene), making it difficult to differentiate between different diesel−kerosene blends based on droplet sliding. Even though 2 μL droplets displayed much larger differences in sliding angles (i.e., 26° difference between diesel and kerosene) compared to 5 μL droplets, their lower sliding velocities led to longer detection times, making them impractical for rapid detection. Furthermore, smaller droplet volumes display higher evaporation rates (due to higher surface-to-volume ratio),[39−41] which may produce inconsistent results due to changes in droplet volume, especially with volatile fuels like diesel and kerosene.

To demonstrate rapid fuel adulteration detection, we sequentially placed 5 μL droplets of diesel−kerosene blends with 5, 10, and 25% kerosene concentrations on our device with OTS-modified glass slides on wedges having 15, 20, and 25° tilt angles. The droplets of diesel + 5% kerosene remained adhered on wedges with 15 and 20° tilt angles, while they slid down the wedge with 25° tilt angle. This is because the sliding angle of diesel + 5% kerosene droplets ($\omega = 21°$) on OTS-modified glass slides is higher than 15 and 20° (i.e., $\omega > \alpha$) but lower than 25° (i.e., $\omega < \alpha$; see Figure 3d). The droplets of diesel + 10% kerosene ($\gamma_{lv} = 23.9$ mN m^{-1}) remained adhered on the wedge with 15° tilt angle, while they slid down the wedges with 20 and 25° tilt angles. This is because the sliding angle of diesel + 10% kerosene droplets ($\omega = 18°$) on OTS-modified glass slides is higher than 15° (see Figure 3e). The droplets of diesel + 25% kerosene ($\gamma_{lv} = 22.3$ mN m^{-1}) slid down all the three wedges because their tilt angles are higher than sliding angle of diesel + 25% kerosene blend ($\omega = 12°$) on OTS-modified glass slides (see Figure 3f and Movie S1). Thus, leveraging our knowledge of diesel−kerosene blend droplet mobility on OTS-modified glass slides, we can easily detect and approximately estimate diesel adulteration even at kerosene concentrations as low as 5%. To put this into context, diesel adulteration is typically as high as 35−50% kerosene.[7,8] In a similar manner, this strategy can be extended to other liquid systems for developing inexpensive and field-deployable devices that can rapidly detect compositional changes.

Furthermore, we investigated the durability (i.e., retention of slipperiness) of OTS-modified surfaces by measuring sliding angles of 20 μL of water and diesel droplets on OTS-modified glass slides after exposing the surfaces to sunlight for 1 day, to steam (at 100 °C and 1 atm) for 1 day, and sliding thousands of water and diesel droplets past the surface (see Supporting Information, Section S7). Our results indicate that OTS-modified surfaces retained their slipperiness even after 1 day exposure to sunlight (see Figure S4a) and 1 day exposure to steam (see Figure S4b), and even after 100,000 water and diesel droplets slid past the surface (see Figure S4c). While these results demonstrate the reusability of our OTS-modified surfaces, a more comprehensive study is necessary to exhaustively quantify the durability of these surfaces for their practical use in detecting fuel adulteration.

CONCLUSIONS

In this work, we developed a simple, inexpensive, and field-deployable device to rapidly detect fuel adulteration. The working principle of our device is identifying the changes in mobility of fuel droplets on non-textured and non-polar solid surfaces. We elucidated the working principle of our device by investigating droplet mobility of multiple liquid systems (i.e., water−SDS mixtures, water−ethanol mixtures, and homologous series of alkanes), including diesel−kerosene blends on non-textured and non-polar solid surfaces with different chemical (i.e., surface chemistry) and physical (i.e., surface roughness) properties. We demonstrated a rapid detection of fuel (i.e., diesel) adulteration even at subsidized fuel (i.e., kerosene) concentrations, an order of magnitude below typical adulteration concentrations. We envision that our inexpensive, easy-to-use, and field-deployable device as well as the design strategy will pave the way for novel fuel quality sensors.

ASSOCIATED CONTENT

Supporting Information

The Supporting Information is available free of charge at https://pubs.acs.org/doi/10.1021/acs.langmuir.3c00578.

Materials and methods; characterization of surface chemistry; sliding angles of different liquid systems on OTS- and FDTS-modified silicon wafers; sliding angles of diesel−kerosene blends on OTS-modified substrates; contact angles and contact angle hysteresis of diesel−kerosene blends; fabrication of 3D-printed fuel adulteration detection devices; and durability of OTS-modified surfaces (PDF)

Mobility of 5 μL diesel−kerosene blend droplets on OTS-modified glass slides tilted at 15, 20, and 25° on our fuel adulteration detection device (MP4)

AUTHOR INFORMATION

Corresponding Author

Arun K. Kota − *Department of Mechanical and Aerospace Engineering, North Carolina State University, Raleigh, North Carolina 27695, United States;* orcid.org/0000-0001-9061-7896; Email: akota2@ncsu.edu

Authors

Sanli Movafaghi − *Department of Mechanical Engineering, Colorado State University, Fort Collins, Colorado 80523, United States*

Sravanthi Vallabhuneni − *Department of Mechanical and Aerospace Engineering, North Carolina State University, Raleigh, North Carolina 27695, United States;* orcid.org/0000-0002-4065-3466

Wei Wang − *Department of Mechanical, Aerospace, and Biomedical Engineering, University of Tennessee Knoxville, Knoxville, Tennessee 37996, United States;* orcid.org/0000-0002-1260-2098

Shantanu Jathar − *Department of Mechanical Engineering, Colorado State University, Fort Collins, Colorado 80523, United States;* orcid.org/0000-0003-4106-2358

Complete contact information is available at: https://pubs.acs.org/10.1021/acs.langmuir.3c00578

Author Contributions

The manuscript was written through contributions of all authors. All authors have given approval to the final version of the manuscript.

Notes

The authors declare no competing financial interest.

https://doi.org/10.1021/acs.langmuir.3c00578
Langmuir 2023, 39, 9044−9050

■ ACKNOWLEDGMENTS

A.K.K. gratefully acknowledges financial support under award 1947454 from the National Science Foundation and under awards R01HL135505 and R21EB033960 from the National Institutes of Health.

■ REFERENCES

(1) Arze del Granado, F. J.; Coady, D.; Gillingham, R. The unequal benefits of fuel subsidies: A review of evidence for developing countries. *World Dev.* **2012**, *40*, 2234−2248.
(2) Gangopadhyay, S.; Ramaswami, B.; Wadhwa, W. Reducing subsidies on household fuels in India: how will it affect the poor? *Energy Policy* **2005**, *33*, 2326−2336.
(3) Pitt, M. M. Equity, externalities and energy subsidies The case of kerosine in Indonesia. *J. Dev. Econ.* **1985**, *17*, 201−217.
(4) Gawande, A. P.; Kaware, J. Fuel adulteration consequences in India: a review. *Sci. Rev. Chem. Commun.* **2013**, *3*, 161−171.
(5) Rao, N. D. Kerosene subsidies in India: When energy policy fails as social policy. *Energy Sustainable Dev.* **2012**, *16*, 35−43.
(6) Shenoy, B. V. Lessons learned from attempts to reform India's kerosene subsidy. *SSRN* **2010**, 1573587.
(7) Yadav, S. R.; Murthy, V.; Mishra, D.; Baral, B. Estimation of petrol and diesel adulteration with kerosene and assessment of usefulness of selected automobile fuel quality test parameters. *Int. J. Environ. Sci. Technol.* **2005**, *1*, 253−255.
(8) Vempatapu, B. P.; Tripathi, D.; Kumar, J.; Kanaujia, P. K. Determination of kerosene as an adulterant in diesel through chromatography and high-resolution mass spectrometry. *SN Appl. Sci.* **2019**, *1*, 614.
(9) Bhowmik, S.; Paul, A.; Panua, R.; Ghosh, S. K. Performance, combustion and emission characteristics of a diesel engine fueled with diesel-kerosene-ethanol: A multi-objective optimization study. *Energy* **2020**, *211*, 118305.
(10) Vempatapu, B. P.; Kanaujia, P. K. Monitoring petroleum fuel adulteration: A review of analytical methods. *Trends Anal. Chem.* **2017**, *92*, 1−11.
(11) Bharath, L. V.; Himanth, M. Review on the Detection of Fuel Adulteration through Sensor based Techniques. *Int. J. Sci. Res. Publ.* **2017**, *7*, 447−451.
(12) Teixeira, L. S.; Oliveira, F. S.; dos Santos, H. C.; Cordeiro, P. W.; Almeida, S. Q. Multivariate calibration in Fourier transform infrared spectrometry as a tool to detect adulterations in Brazilian gasoline. *Fuel* **2008**, *87*, 346−352.
(13) Wiziack, N. K. L.; Catini, A.; Santonico, M.; D'amico, A.; Paolesse, R.; Paterno, L. G.; Fonseca, F. J.; Di Natale, C. A sensor array based on mass and capacitance transducers for the detection of adulterated gasolines. *Sens. Actuators, B* **2009**, *140*, 508−513.
(14) Furmidge, C. Studies at phase interfaces. I. The sliding of liquid drops on solid surfaces and a theory for spray retention. *J. Colloid Sci.* **1962**, *17*, 309−324.
(15) Kota, A. K.; Li, Y.; Mabry, J. M.; Tuteja, A. Hierarchically structured superoleophobic surfaces with ultralow contact angle hysteresis. *Adv. Mater.* **2012**, *24*, 5838−5843.
(16) Kawasaki, K. Study of wettability of polymers by sliding of water drop. *J. Colloid Sci.* **1960**, *15*, 402−407.
(17) Buzágh, A.; Wolfram, E. Bestimmung der Haftfähigkeit von Flüssigkeiten an festen Körpern mit der Abreißwinkelmethode. II. *Kolloid-Z.* **1958**, *157*, 50−53.
(18) Bikerman, J. Sliding of drops from surfaces of different roughnesses. *J. Colloid Sci.* **1950**, *5*, 349−359.
(19) Extrand, C. W.; Kumagai, Y. Liquid drops on an inclined plane: the relation between contact angles, drop shape, and retentive force. *J. Colloid Interface Sci.* **1995**, *170*, 515−521.
(20) Tang, S.; Bhimavarapu, Y.; Gulec, S.; Das, R.; Liu, J.; N'guessan, H.; Whitehead, T.; Yao, C. W.; Tadmor, R. Droplets sliding down a vertical surface under increasing horizontal forces. *Langmuir* **2019**, *35*, 8191−8198.
(21) McHale, G.; Gao, N.; Wells, G. G.; Barrio-Zhang, H.; Ledesma-Aguilar, R. Friction coefficients for droplets on solids: the liquid−solid Amontons' laws. *Langmuir* **2022**, *38*, 4425−4433.
(22) Wang, L.; McCarthy, T. J. Covalently attached liquids: instant omniphobic surfaces with unprecedented repellency. *Angew. Chem., Int. Ed.* **2016**, *55*, 244−248.
(23) Singh, N.; Kakiuchida, H.; Sato, T.; Hönes, R.; Yagihashi, M.; Urata, C.; Hozumi, A. Omniphobic metal surfaces with low contact angle hysteresis and tilt angles. *Langmuir* **2018**, *34*, 11405−11413.
(24) Vahabi, H.; Vallabhuneni, S.; Hedayati, M.; Wang, W.; Krapf, D.; Kipper, M. J.; Miljkovic, N.; Kota, A. K. Designing non-textured, all-solid, slippery hydrophilic surfaces. *Matter* **2022**, *5*, 4502−4512.
(25) Park, J.; Urata, C.; Masheder, B.; Cheng, D. F.; Hozumi, A. Long perfluoroalkyl chains are not required for dynamically oleophobic surfaces. *Green Chem.* **2013**, *15*, 100−104.
(26) Eaton, D. F.; Smart, B. E. Are fluorocarbon chains stiffer than hydrocarbon chains? Dynamics of end-to-end cyclization in a C8F16 segment monitored by fluorescence. *J. Am. Chem. Soc.* **1990**, *112*, 2821−2823.
(27) Rodriguez-Parada, J.; Kaku, M.; Sogah, D. Monolayers and Langmuir-Blodgett films of poly (N-acylethylenimines) with hydrocarbon and fluorocarbon side chains. *Macromolecules* **1994**, *27*, 1571−1577.
(28) Overney, R. M.; Meyer, E.; Frommer, J.; Brodbeck, D.; Lüthi, R.; Howald, L.; Giintherodt, H. J.; Fujihira, M.; Takano, H.; Gotoh, Y. Friction measurements on phase-separated thin films with a modified atomic force microscope. *Nature* **1992**, *359*, 133−135.
(29) Barton, S. W.; Goudot, A.; Bouloussa, O.; Rondelez, F.; Lin, B.; Novak, F.; Acero, A.; Rice, S. A. Structural transitions in a monolayer of fluorinated amphiphile molecules. *J. Chem. Phys.* **1992**, *96*, 1343−1351.
(30) Newby, B. M. Z.; Chaudhury, M. K.; Brown, H. R. Macroscopic evidence of the effect of interfacial slippage on adhesion. *Science* **1995**, *269*, 1407−1409.
(31) Chang, C. C.; Wu, C. J.; Sheng, Y. J.; Tsao, H. K. Anti-smudge behavior of facilely fabricated liquid-infused surfaces with extremely low contact angle hysteresis property. *RSC Adv.* **2016**, *6*, 19214−19222.
(32) Yong, J.; Yang, Q.; Chen, F.; Zhang, D.; Du, G.; Bian, H.; Si, J.; Hou, X. Bioinspired superhydrophobic surfaces with directional Adhesion. *RSC Adv.* **2014**, *4*, 8138−8143.
(33) Buck, R. C.; Franklin, J.; Berger, U.; Conder, J. M.; Cousins, I. T.; De Voogt, P.; Jensen, A. A.; Kannan, K.; Mabury, S. A.; van Leeuwen, S. P. Perfluoroalkyl and polyfluoroalkyl substances in the environment: terminology, classification, and origins. *Integr. Environ. Assess. Manage.* **2011**, *7*, 513−541.
(34) Haukås, M.; Berger, U.; Hop, H.; Gulliksen, B.; Gabrielsen, G. W. Bioaccumulation of per-and polyfluorinated alkyl substances (PFAS) in selected species from the Barents Sea food web. *Environ. Pollut.* **2007**, *148*, 360−371.
(35) Blum, A.; Balan, S. A.; Scheringer, M.; Trier, X.; Goldenman, G.; Cousins, I. T.; Diamond, M.; Fletcher, T.; Higgins, C.; Lindeman, A. E.; Peaslee, G.; et al. The Madrid statement on poly-and perfluoroalkyl substances (PFASs). *Environ. Health Perspect.* **2015**, *123*, A107−A111.
(36) Miwa, M.; Nakajima, A.; Fujishima, A.; Hashimoto, K.; Watanabe, T. Effects of the surface roughness on sliding angles of water droplets on superhydrophobic surfaces. *Langmuir* **2000**, *16*, 5754−5760.
(37) Cassie, A. B. D.; Baxter, S. Wettability of porous surfaces. *Trans. Faraday Soc.* **1944**, *40*, 546−551.
(38) Wenzel, R. N. Surface roughness and contact angle. *J. Phys. Chem. A* **1949**, *53*, 1466−1467.
(39) Li, X.; Shang, Y.; Yan, Y.; Yang, L.; Tu, J. Modelling of evaporation of cough droplets in inhomogeneous humidity fields using the multi-component Eulerian-Lagrangian approach. *Build. Environ.* **2018**, *128*, 68−76.
(40) Madero, J. E.; Yi, F.; Axelbaum, R. L. PDPA Studies during Oxy-Combustion of Ethanol Heavily Diluted in Water. In *Heterogenous Sprays & Droplets, 9th U. S. National Combustion Meeting*, Cincinnati, Ohio, May 17−20, 2015; pp 1−8.

https://doi.org/10.1021/acs.langmuir.3c00578
Langmuir 2023, 39, 9044−9050

(41) Stadnytskyi, V.; Bax, C. E.; Bax, A.; Anfinrud, P. The airborne lifetime of small speech droplets and their potential importance in SARS-CoV-2 transmission. *Proc. Natl. Acad. Sci. U.S.A.* **2020**, *117*, 11875−11877.

https://doi.org/10.1021/acs.langmuir.3c00578
Langmuir 2023, 39, 9044−9050

Rapid and On-site Detection of Fuel Adulteration

Sanli Movafaghi[a], Sravanthi Vallabhuneni[b], Wei Wang[c], Shantanu Jathar[a], and Arun K. Kota[b*]

[a]Department of Mechanical Engineering, Colorado State University, Fort Collins, CO 80523, United States

[b]Department of Mechanical and Aerospace Engineering, North Carolina State University, Raleigh, NC 27695, United States

[c]Department of Mechanical, Aerospace, and Biomedical Engineering, University of Tennessee Knoxville, TN 37996, United States

[*]E-mail: akota2@ncsu.edu

KEYWORDS: fuel adulteration, droplet mobility, slippery, on-site detection, 3D printing

Section 1. Materials and Methods

Fabrication of OTS-modified and FDTS-modified surfaces: Silicon wafers (<1 0 0> orientation; University Wafers) and glass slides (Fisher Scientific) were cleaned by rinsing thoroughly with acetone (Fisher Scientific) and DI water, and then dried with nitrogen. The cleaned substrates were exposed to oxygen plasma (Plasma Etch PE-25) for 15 min for hydroxylation. To prepare OTS-modified surfaces, the hydroxylated substrates were immersed in a solution consisting of 15 mL toluene (Fisher Scientific), 12 µL of hydrochloric acid (Fisher Scientific), and 16 µL of octadecyltrichlorosilane (OTS; Gelest) for 2 hours at room temperature (see Figure S1). To prepare FDTS-modified surfaces, the hydroxylated substrates were immersed in a solution consisting of 15 mL toluene (Fisher Scientific), 12 µL of hydrochloric acid (Fisher Scientific), and 16 µL of heptadecafluoro-1,1,2,2-tetrahydrodecyl trichlorosilane (FDTS; Gelest) for 2 hours at room temperature (see Figure S1). Finally, the silanized samples were cleaned by rinsing thoroughly with anhydrous toluene, DI water and ethanol (Fisher) sequentially, and then dried with nitrogen.

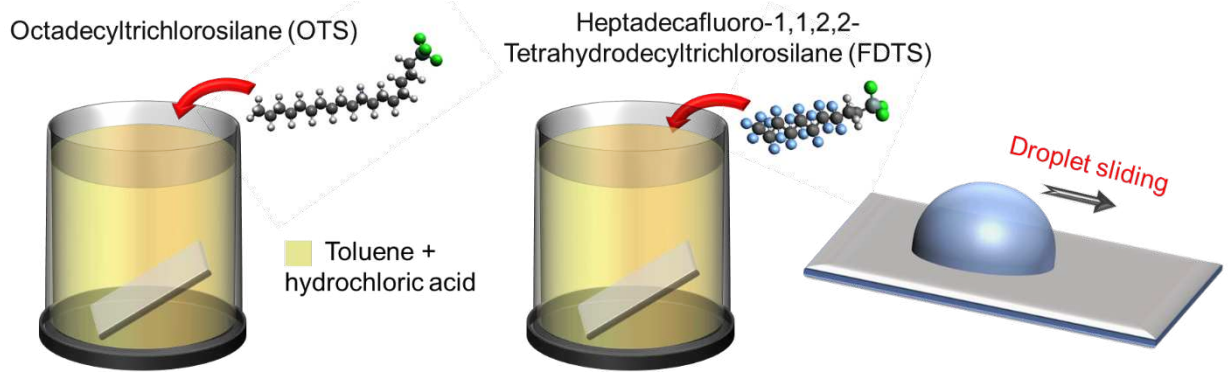

Figure S1. Schematics depicting the surface modification of substrates using OTS and FDTS.

Contact angle, sliding angle and surface tension measurements: The contact angles and sliding angles were measured with sessile droplets and liquid surface tension was measured with pendant droplets using a contact angle goniometer/tensiometer (Ramé-Hart 200-F1). At least three measurements were performed on each surface at spatially distinct locations. The standard

deviation is reported as error with contact angle and sliding angle measurements. The error in surface tension is ±0.2 mN m^{-1}.

Ellipsometry measurements: The thickness of OTS and FDTS brush layers on our surfaces were determined using a variable angle spectroscopic ellipsometer (VASE-VB-250). A spectral scan of the surface was collected between 500 nm and 900 nm for an incident angle between 55° and 75° with an increment of 5°. The thickness of OTS/FDTS brush layers (refractive index ≈ 1.46) were determined using a three-layer planar model (air/brush/silica). For all our ellipsometry data, at least three measurements were conducted on different samples. Our ellipsometry results indicate that the average thickness of both OTS and FDTS-modified surfaces is ≈ 1 nm.

Surface roughness measurements: The root mean square roughness R_{rms} of the silicon wafers and glass slides was measured using an optical profilometer (Zygo Zescope). At least three measurements were performed on each surface at spatially distinct locations. The standard deviation is reported as error with all measurements. Our optical profilometry results indicate that the R_{rms} of our surfaces did not change significantly upon surface modification with OTS or FDTS.

Characterization of surface chemistry: The surface chemistry of substrates was characterized using X-ray photo-electron spectroscopy (XPS; Physical Electronics PHI-5800 spectrometer). XPS was conducted using a monochromatic Al Ka X-ray source operated at 15 kV, and photoelectrons were collected at a takeoff angle of 45° relative to the sample surface. XPS data was acquired from at least 5 spatially different locations on the surface and the spectral analysis was conducted using PHI Multipak software.

Section 2. Characterization of surface chemistry

X-ray photo-electron spectroscopy (XPS) was conducted to investigate the surface chemistry of unmodified, OTS-modified and FDTS-modified silicon wafers. The full survey spectra and high-resolution C1s XPS spectra are reported in Figure S2.

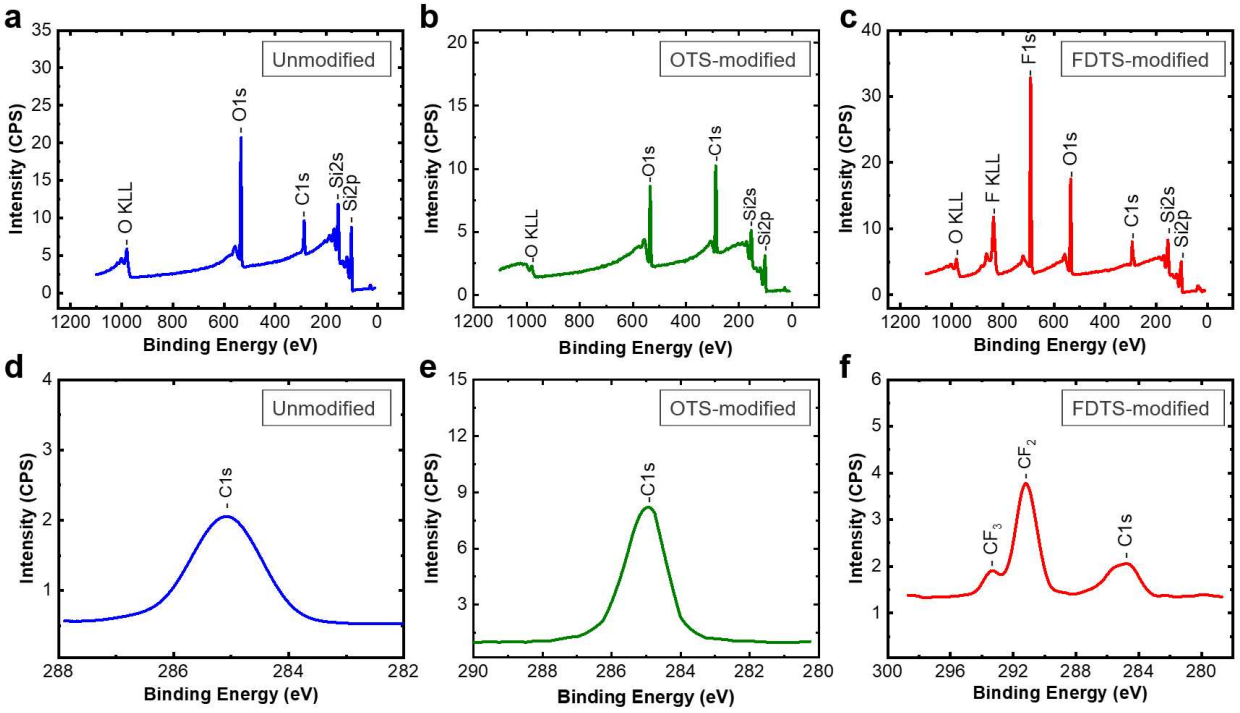

Figure S2. Full survey XPS spectra on a) unmodified, b) OTS-modified and c) FDTS-modified silicon wafers. High-resolution C1s XPS spectra of d) unmodified, e) OTS-modified and f) FDTS-modified silicon wafers.

Section 3. Sliding angles of different liquid systems on OTS and FDTS-modified silicon wafers

The sliding angles of water-SDS mixtures, water-ethanol mixtures, and homologous series of alkanes with different droplet volumes on OTS and FDTS-modified silicon wafers are reported in Table S1. For all sliding angles, the measurements were conducted on at least three different samples and the standard deviation is reported as the error with all measurements.

Table S1. Sliding angles of 20 μL, 10 μL, and 2 μL droplets of water-SDS mixtures, water-ethanol mixtures, and homologous series of alkanes on OTS and FDTS-modified silicon wafers

Liquid	**Droplet volume (μL)**	**Sliding angle (°)**	
		OTS	**FDTS**
Water	20	10±0.5	16±0.8
	10	15±0.5	25±0.8
	2	85±2.5	No sliding
1 mM SDS	20	10±0.5	13±0.8
	10	15±0.5	23±0.8
	2	69±2	81±2.5
2 mM SDS	20	10±0.5	11±0.8
	10	14±0.5	19±0.8
	2	54±2	69±2
3 mM SDS	20	9±0.5	10±0.8
	10	14±0.5	17±0.8
	2	48±1.5	53±2
4 mM SDS	20	9±0.5	9±0.5

Table S1 (contd.). Sliding angles of 20 μL, 10 μL, and 2 μL droplets of water-SDS mixtures, water-ethanol mixtures, and homologous series of alkanes on OTS and FDTS-modified silicon wafers

Liquid	Droplet volume (μL)	Sliding angle (°)	
		OTS	FDTS
4 mM SDS	10	13±0.5	17±0.5
	2	35±1.5	46±2
5 mM SDS	20	8±0.5	8±0.5
	10	13±0.5	15±0.8
	2	28±1.5	33±1.5
6 mM SDS	20	6±0.5	8±0.5
	10	11±0.5	13±0.8
	2	24±1.5	30±1.5
Water+20% Ethanol	20	9±0.5	14±0.8
	10	13±0.8	23±0.8
	2	47±2	85±2.5
Water+40% Ethanol	20	8±0.5	14±0.5
	10	11±0.8	22±0.8
	2	26±2	57±2
Water+50% Ethanol	20	6±0.5	13±0.8
	10	8±0.5	22±0.8
	2	15±1.5	47±1.5
Water+60% Ethanol	20	4.5±0.5	10±0.8

Table S1 (contd.). Sliding angles of 20 μL, 10 μL, and 2 μL droplets of water-SDS mixtures, water-ethanol mixtures, and homologous series of alkanes on OTS and FDTS-modified silicon wafers

Liquid	Droplet volume (μL)	Sliding angle (°)	
		OTS	FDTS
Water+60% Ethanol	10	6±0.47	21±0.8
	2	10±0.8	36±1.5
Water+80% Ethanol	20	3.5±0.5	8.5±0.5
	10	5±0.5	19±0.8
	2	8±0.5	29±1.5
Ethanol	20	3±0.5	7±0.5
	10	4±0.5	15±0.8
	2	6±0.5	20±1.5
Hexadecane	20	2±0.5	13±0.8
	10	4±0.5	23±0.8
	2	10±0.8	No sliding
Tetradecane	20	1.5±0.5	8±0.5
	10	3±0.5	17±0.8
	2	6±0.8	79±2.5
Dodecane	20	1±0.5	7±0.5
	10	2±0.5	15±0.8
	2	5±0.8	56±2
Decane	20	0.5±0.5	7±0.5

Table S1 (contd.). Sliding angles of 20 μL, 10 μL, and 2 μL droplets of water-SDS mixtures, water-ethanol mixtures, and homologous series of alkanes on OTS and FDTS-modified silicon wafers

Liquid	Droplet volume (μL)	Sliding angle (°)	
		OTS	FDTS
Decane	10	1.5±0.5	14±0.8
	2	4±0.5	48±1.5
Octane	20	0.5±0.5	5±0.5
	10	0.5±0.5	11±0.8
	2	4±0.5	41±1.5

Section 4. Sliding angles of diesel-kerosene blends on OTS-modified substrates

The sliding angles of diesel-kerosene blends with different droplet volumes on OTS-modified silicon wafers and OTS-modified glass slides are reported in Table S2. For all sliding angles, the measurements were conducted on at least three different samples and the standard deviation is reported as the error with all measurements.

Table S2. Sliding angles of 20 μL, 10 μL, 5 μL, and 2 μL droplets of diesel-kerosene blends on OTS-modified silicon wafers and OTS-modified glass slides

Liquid (Surface tension)	**Droplet volume (μL)**	**Sliding angle (°)**	
		Silicon	**Glass**
Diesel ($25.8\ mN\ m^{-1}$)	20	4±0.5	10±0.5
	10	6±0.5	16±0.5
	5	11±0.5	25±0.8
	2	25±0.8	47±0.8
Diesel+5% Kerosene ($24.5\ mN\ m^{-1}$)	20	4±0.5	9±0.5
	10	5±0.5	13±0.5
	5	10±0.5	21±0.8
	2	23±0.8	42±0.8
Diesel+10% Kerosene ($23.9\ mN\ m^{-1}$)	20	3±0.5	8±0.5
	10	5±0.5	11±0.5
	5	10±0.5	18±0.8
	2	22±0.5	38±0.8

Table S2 (contd.). Sliding angles of 20 μL, 10 μL, 5 μL, and 2 μL droplets of diesel-kerosene blends on OTS-modified silicon wafers and OTS-modified glass slides

Liquid (Surface tension)	**Droplet volume (μL)**	**Sliding angle (°)**	
		Silicon	**Glass**
Diesel+25% Kerosene ($22.3\ mN\ m^{-1}$)	20	3±0.5	7±0.5
	10	4±0.5	10±0.5
	5	8±0.5	12±0.8
	2	19±0.5	33±0.8
Diesel+50% Kerosene ($21.2\ mN\ m^{-1}$)	20	2±0.5	6±0.5
	10	4±0.5	9±0.5
	5	8±0.5	10±0.5
	2	15±0.5	31±0.8
Diesel+75% Kerosene ($20.6\ mN\ m^{-1}$)	20	2±0.5	5±0.5
	10	4±0.5	8±0.5
	5	5.5±0.5	9±0.8
	2	11±0.5	27±0.8
Kerosene ($20.1\ mN\ m^{-1}$)	20	1±0.5	5±0.5
	10	3±0.5	7±0.5
	5	5±0.5	8±0.5
	2	9±0.5	21±0.8

Section 5. Contact angles and contact angle hysteresis of diesel-kerosene blends

The advancing contact angle (θ_{adv}) and receding contact angle (θ_{rec}) and contact angle hysteresis ($\Delta\theta = \theta_{adv} - \theta_{rec}$) of diesel-kerosene blends on OTS-modified glass slides are reported in Table S3. All measurements were conducted on at least three different samples and the standard deviation is reported as the error with all the data.

Table S3. Contact angles and contact angle hysteresis of diesel-kerosene blends.

Liquid	$\boldsymbol{\theta_{adv}}$ **(°)**	$\boldsymbol{\theta_{rec}}$ **(°)**	$\boldsymbol{\Delta\theta}$ **(°)**
Diesel	38±0.5	27±0.5	11
Diesel+5% Kerosene	37±0.8	27±0.8	10
Diesel+10% Kerosene	37±0.5	28±0.5	9
Diesel+25% Kerosene	35±0.8	28±0.5	7
Diesel+50% Kerosene	32±0.5	26±0.5	6
Diesel+75% Kerosene	27±0.8	22±0.8	5
Kerosene	23±0.8	18±0.8	5

Section 6. Fabrication of 3D printed fuel adulteration detection device

Our fuel adulteration detection device was fabricated with acrylonitrile butadiene styrene using a 3D printer (uPrint SE, Stratasys). The device consists of multiple domains that can hold flat substrates (e.g., OTS-modified glass slides) at different tilt angles. An image of the 3D printed fuel adulteration detection device is presented in Figure S3.

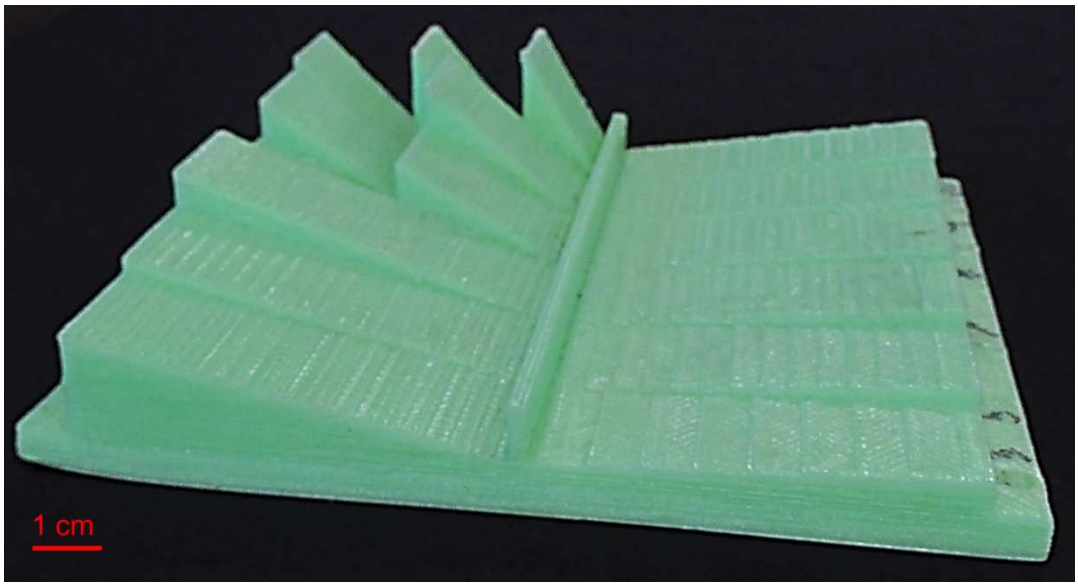

Figure S3. 3D printed fuel adulteration detection device.

Section 7. Durability of OTS-modified surfaces

We investigated the durability (i.e., retention of slipperiness) of our OTS-modified glass slides by measuring sliding angles of 20 μL water and diesel droplets after exposing the surfaces to sunlight for 1 day, to steam (at 100°C and 1 atm) for 1 day and sliding thousands of water and diesel droplets past the surface. Our results indicate that that OTS-modified surfaces retained their slipperiness (i.e., no significant change in sliding angles) even after 1 day exposure to sunlight (see Figure S4a) and 1 day exposure to steam (see Figure S4b) and even after 100,000 water and diesel droplets slid past the surface (see Figure S4c). While these results demonstrate the reusability of our OTS-modified surfaces, a more comprehensive study is necessary to exhaustively quantify the durability of these surfaces for their practical use.

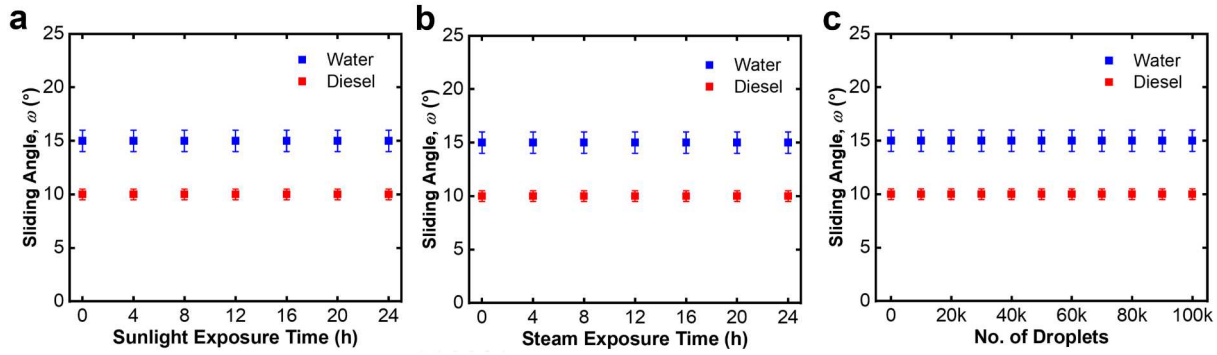

Figure S4. Sliding angles of 20 μL water and diesel droplets on OTS-modified glass slides after exposing the surfaces a) to sunlight for 1 day, b) to steam for 1 day and c) sliding thousands of water and diesel droplets past the surface.

Movie Legends

Movie S1. Mobility of 5 μL diesel-kerosene blend droplets on OTS-modified glass slides tilted at 15°, 20° and 25° on our fuel adulteration detection device.